

Simultaneous occurrence of distinct symmetries in nuclei

A. Leviatan

Racah Institute of Physics, The Hebrew University, Jerusalem 91904, Israel

E-mail: ami@phys.huji.ac.il

Abstract. We show that distinct emergent symmetries, such as partial dynamical symmetry and quasi dynamical symmetry, can occur simultaneously in the same or different eigenstates of the Hamiltonian. Implications for nuclear spectroscopy in the rare-earth region and for first-order quantum phase transitions between spherical and deformed shapes, are considered.

1. Introduction

Symmetries play an important role in the understanding of complex systems. However, complete dynamical symmetries (DS) are manifest in only a few nuclei. Generic Hamiltonians involve interaction terms with competing incompatible symmetries, which break the DS. More often one finds that the assumed symmetry is not obeyed uniformly, *i.e.*, is fulfilled by some of the states but not by others. The need to address such situations, but still preserve important symmetry remnants, has led to the introduction of partial dynamical symmetry (PDS) [1]. For the latter, only part of the eigenspectrum observes a symmetry and retains good quantum numbers and/or complete solvability. Various types of PDS were proposed and extensive tests have provided empirical evidence for their relevance to a broad range of nuclei, *e.g.*, in the rare-earth [2–4], platinum [5, 6] and actinide [7] regions, in light nuclei [8] and in semi-magic nuclei [9]. In parallel, the notion of quasi dynamical symmetry (QDS) was introduced and discussed in the context of nuclear models [10, 11]. It expresses the tendency of a Hamiltonian to exhibit characteristic properties of the closest DS, for a certain range of its parameters. This “apparent” (but broken) symmetry, is due to a coherent mixing of representations in selected states, which share a common intrinsic structure.

The concept of PDS reflects the purity of selected states, as opposed to QDS which reflects a coherent mixing. Up to now, these two symmetry concepts have been considered to be unrelated. In the present contribution, we establish a linkage between them and show that both can occur simultaneously in the same or in different eigenstates of the Hamiltonian. Implications for the spectroscopy of rare-earth nuclei [12] and for shape-phase transitions [13–15] are considered.

2. The interacting boson model: test ground for competing symmetries

The interacting boson model (IBM) [16] provides a convenient framework for exploring the role of symmetries in nuclei. It has been widely used to describe quadrupole collective states in nuclei in terms of N monopole (s^\dagger) and quadrupole (d^\dagger) bosons, representing valence nucleon pairs. The model has $U(6)$ as a spectrum generating algebra and exhibits three DS limits associated

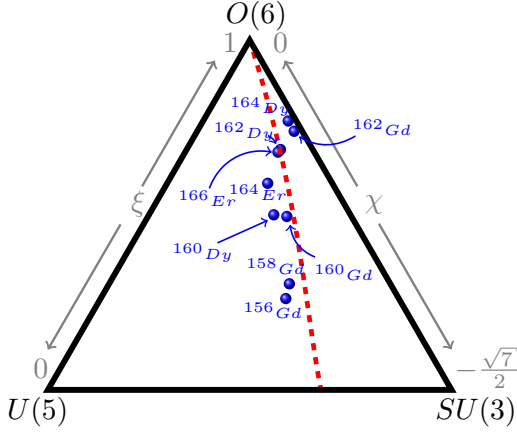


Figure 1. The ECQF symmetry triangle with the position of the rare-earth nuclei of Table 1 indicated by bullets. The calculated (for $N = 60$) red dashed line, correspond to a region of an approximate ground-state $O(6)$ symmetry, exemplifying an $O(6)$ -PDS, as discussed in Section 3. From [20].

with the following chains of nested subalgebras,

$$U(6) \supset U(5) \supset O(5) \supset O(3) \quad |N, n_d, \tau, n_\Delta, L\rangle \quad (1a)$$

$$U(6) \supset SU(3) \supset O(3) \quad |N, (\lambda, \mu), K, L\rangle \quad (1b)$$

$$U(6) \supset O(6) \supset O(5) \supset O(3) \quad |N, \sigma, \tau, n_\Delta, L\rangle . \quad (1c)$$

The indicated basis states are classified by quantum numbers which are the labels of irreducible representation (irreps) of the algebras in each chain. These solvable limits correspond to known benchmarks of the geometric description of nuclei, involving vibrational [$U(5)$], γ -soft [$O(6)$], and rotational [$SU(3)$] types of dynamics. This identification is consistent with the geometric visualization of the model. The latter is obtained by an energy surface, $E(\beta, \gamma)$, defined by the expectation value of the Hamiltonian in the coherent (intrinsic) state [17],

$$|\beta, \gamma; N\rangle = (N!)^{-1/2} (b_c^\dagger)^N |0\rangle , \quad (2)$$

where, $b_c^\dagger \propto \beta \cos \gamma d_0^\dagger + \beta \sin \gamma (d_2^\dagger + d_{-2}^\dagger)/\sqrt{2} + s^\dagger$. Here (β, γ) are quadrupole shape parameters whose values, $(\beta_{eq}, \gamma_{eq})$, at the global minimum of $E(\beta, \gamma)$ define the equilibrium shape for a given Hamiltonian. For one- and two-body interactions, the energy surface is of the form

$$E(\beta, \gamma) \propto (1 + \beta^2)^{-2} \beta^2 [a - b\beta \cos 3\gamma + c\beta^2] . \quad (3)$$

The shape can be spherical ($\beta = 0$) or deformed ($\beta > 0$) with $\gamma = 0$ (prolate), $\gamma = \pi/3$ (oblate), or γ -independent. The equilibrium deformations associated with the DS limits are $\beta_{eq} = 0$ for $U(5)$, $(\beta_{eq} = \sqrt{2}, \gamma_{eq} = 0)$ for $SU(3)$ and $(\beta_{eq} = 1, \gamma_{eq} \text{ arbitrary})$ for $O(6)$.

The extended consistent-Q formalism (ECQF) [18] of the IBM, uses the same quadrupole operator, $\hat{Q}^\chi = d^\dagger s + s^\dagger \tilde{d} + \chi (d^\dagger \tilde{d})^{(2)}$, in the E2 transition operator and in the Hamiltonian,

$$\hat{H}_{ECQF} = \omega \left[(1 - \xi) \hat{n}_d - \frac{\xi}{4N} \hat{Q}^\chi \cdot \hat{Q}^\chi \right] . \quad (4)$$

Here \hat{n}_d is the d-boson number operator, $\tilde{d}_m = (-)^m d_{-m}$ and the dot implies a scalar product. ξ and χ are the sole structural parameters of the model since ω is a scaling factor. The parameter ranges $0 \leq \xi \leq 1$ and $-\frac{\sqrt{7}}{2} \leq \chi \leq 0$ interpolate between the $U(5)$, $O(6)$ and $SU(3)$ DS limits, which are reached for $(\xi, \chi) = (0, \chi)$, $(1, 0)$, and $(1, -\frac{\sqrt{7}}{2})$, respectively. It is customary to represent the parameter space by a symmetry triangle [19], shown in Fig. 1, whose vertices correspond to these limits. The ECQF has been used extensively for describing nuclei [21] and it was found that the vast majority of nuclei are best described by ECQF parameters in the interior of the triangle, away from any DS limit. In what follows we examine the $O(6)$ symmetry properties of ground-band states in such nuclei, in the rare-earth region, using \hat{H}_{ECQF} (4).

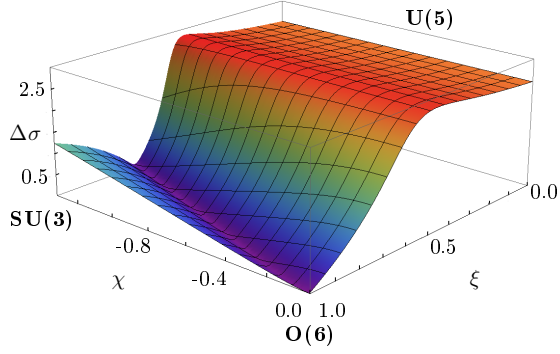


Figure 2. Ground-state ($L=0_1^+$) fluctuations $\Delta\sigma_0$ (5) for \hat{H}_{ECQF} (4) with $N = 14$. The fluctuations vanish at the O(6) DS limit, saturate towards the U(5) DS limit, and are of the order 10^{-2} in the valley. Adapted from [12].

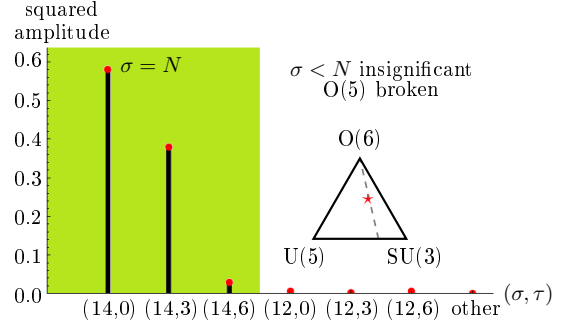


Figure 3. Squared amplitudes C_i^2 in the expansion in the O(6) basis (1c), of the $L=0_1^+$ ground state of the ECQF Hamiltonian (4) with parameters $\xi = 0.84$, $\chi = -0.53$, $N = 14$, appropriate for ^{160}Gd . Adapted from [12].

3. Simultaneous occurrence of O(6)-PDS and SU(3)-QDS in rotational nuclei

Given an eigenstate $|L\rangle$, with angular momentum L , of the ECQF Hamiltonian (4), its expansion in the O(6) DS basis reads $|L\rangle = \sum_i C_i |N, \sigma_i, \tau_i, L\rangle$. The degree of O(6) symmetry of the state $|L\rangle$ is inferred from the fluctuations in σ , calculated as [12],

$$\Delta\sigma_L = \sqrt{\sum_i C_i^2 \sigma_i^2 - \left(\sum_i C_i^2 \sigma_i\right)^2}. \quad (5)$$

If $|L\rangle$ carries an exact O(6) quantum number, σ fluctuations are zero, $\Delta\sigma_L = 0$. If $|L\rangle$ contains basis states with different O(6) quantum numbers, then $\Delta\sigma_L > 0$, indicating that the O(6) symmetry is broken. Note that $\Delta\sigma_L$ also vanishes for a state with a mixture of components with the same σ but different O(5) quantum numbers τ , corresponding to a state $|L\rangle$ with good O(6) but mixed O(5) character. $\Delta\sigma_L$ has the same physical content as wave-function entropy.

The fluctuations $\Delta\sigma_L$ can now be examined for the entire parameter space of the ECQF Hamiltonian (4). Results of this calculation for the ground state, $|L=0_1^+\rangle$, with $N = 14$, are shown in Fig. 2. At the O(6) DS limit ($\xi = 1$, $\chi = 0$), $\Delta\sigma_0 \equiv \Delta\sigma_{L=0_1}$ vanishes per construction whereas it is greater than zero for all other parameter pairs. Towards the U(5) DS limit ($\xi = 0$), the fluctuations reach a saturation value of $\Delta\sigma_0 \approx 2.47$. At the SU(3) DS limit ($\xi = 1$, $\chi = -\frac{\sqrt{7}}{2}$) the fluctuations are $\Delta\sigma_0 \approx 1.25$. Surprisingly, one recognizes a valley of almost vanishing $\Delta\sigma_0$ values, two orders of magnitude lower than at saturation. This region (depicted by a red dashed arc in the triangle of Fig. 1), represents a parameter range of the IBM, outside the O(6) DS limit, where the ground-state wave function exhibits an exceptionally high degree of purity with respect to the O(6) quantum number σ .

The ground-state wave functions in the valley of low $\Delta\sigma_0$, can be expanded in the O(6)-DS basis (1c). At the O(6) DS limit only one O(6) basis state, with $\sigma = N$ and $\tau = 0$ contributes, while outside this limit the wave function consists of multiple O(6) basis states. Investigation of the wave function for parameter combinations inside the valley reveals an overwhelming dominance of the O(6) basis states with $\sigma = N$. This is seen in Fig. 3 for the ground-state wave function of \hat{H}_{ECQF} (4), with parameter values that apply to the nucleus ^{160}Gd . The $\sigma = N$ states comprise more than 99% of the ground-state wave function at the bottom of the valley and their dominance causes $\Delta\sigma_0$ to be small. At the same time, the O(5) symmetry is broken, as basis states with different quantum number τ contribute significantly to the wave

Table 1. Calculated σ fluctuations $\Delta\sigma_L$, Eq. (5), for rare earth nuclei in the vicinity of the identified region of approximate ground-state-O(6) symmetry [12]. Also shown are the fraction $f_{\sigma=N}^{(L)}$ of O(6) basis states with $\sigma = N$ contained in the $L = 0, 2, 4$ states, members of the ground band. The structure parameters ξ and χ of the ECQF Hamiltonian (4) employed, are taken from [21].

Nucleus	N	ξ	χ	$\Delta\sigma_0$	$f_{\sigma=N}^{(0)}$	$\Delta\sigma_2$	$f_{\sigma=N}^{(2)}$	$\Delta\sigma_4$	$f_{\sigma=N}^{(4)}$
^{156}Gd	12	0.72	-0.86	0.46	95.3%	0.43	95.8%	0.38	96.6%
^{158}Gd	13	0.75	-0.80	0.35	97.2%	0.33	97.5%	0.30	97.9%
^{160}Gd	14	0.84	-0.53	0.19	99.1%	0.19	99.2%	0.17	99.3%
^{162}Gd	15	0.98	-0.30	0.17	99.3%	0.17	99.3%	0.16	99.3%
^{160}Dy	14	0.81	-0.49	0.44	96.2%	0.39	96.4%	0.36	96.8%
^{162}Dy	15	0.92	-0.31	0.07	99.9%	0.07	99.9%	0.06	99.9%
^{164}Dy	16	0.98	-0.26	0.13	99.6%	0.13	99.6%	0.13	99.6%
^{164}Er	14	0.84	-0.37	0.39	96.5%	0.37	96.7%	0.35	97.1%
^{166}Er	15	0.91	-0.31	0.12	99.7%	0.11	99.7%	0.10	99.7%

function. Consequently, the valley can be identified as an entire region in the symmetry triangle with an approximate O(6)-PDS, which means that some of the eigenstates exhibit some of the symmetries in the chain (1c). Outside this valley the ground state is a mixture of several σ values and $\Delta\sigma_0$ increases.

Detailed ECQF fits for energies and electromagnetic transitions of rare-earth nuclei [21], allow one to relate the structure of collective nuclei to the parameter space of the ECQF Hamiltonian (4). From the extracted (ξ, χ) parameters one can calculate the fluctuations $\Delta\sigma_L$ and the fractions $f_{\sigma=N}$ of squared $\sigma = N$ amplitude. Nuclei with $\Delta\sigma_0 < 0.5$ and $f_{\sigma=N} > 95\%$ in the ground-state ($L = 0_1^+$) are listed in Table 1. These quantities are also calculated for yrast states with $L > 0$ and exhibit similar values in each nucleus. It is evident that a large set of rotational rare earth nuclei are located in the valley of small σ fluctuations. They can be identified as candidate nuclei with an approximate O(6)-PDS not only for the ground state, but also for the members of the band built on top of it.

The experimental spectrum of a representative nucleus from Table 1, ^{160}Gd , along with its ECQF description (4), is shown in Fig. 4(a). Figures 4(b) and 4(c) show the decomposition into O(6) and SU(3) basis states, respectively, for yrast states with $L = 0, 2, 4$. It is evident that the SU(3) symmetry is broken, as significant contributions of basis states with different SU(3) quantum numbers (λ, μ) occur. It is also clear from Fig. 4(c) that this mixing occurs in a coherent manner with similar patterns for the different members of the ground-state band. Such coherent mixing is the hallmark of SU(3) QDS [11]. On the other hand, as seen in Fig. 4, the same yrast states with $L = 0, 2, 4$ are almost entirely composed out of O(6) basis states with $\sigma = N = 14$ which implies small fluctuations $\Delta\sigma_L$ (5) and the preservation of O(6) symmetry (but with broken O(5) symmetry) in the ground-state band. Thus an empirically-manifested link is established between SU(3) QDS and O(6) PDS.

The simultaneous occurrence of SU(3)-QDS and O(6)-PDS for members of the ground band, signals the existence of a single intrinsic state with good O(6) character. Such an intrinsic state is the condensate of Eq. (2) with $(\beta = 1, \gamma = 0)$, that has $\sigma = N$. The states projected from it keep exact O(6) symmetry ($\sigma = N$) but break the O(5) symmetry (mixed τ) and have a high overlap with the yrast eigenstates of \hat{H}_{ECQF} (more than 99% for the ground states $L = 0_1^+$). This suggests that the indicated intrinsic state provides a good approximation, in a variational sense, to the ground band of \hat{H}_{ECQF} along the valley of low- $\Delta\sigma_0$. The two extremum

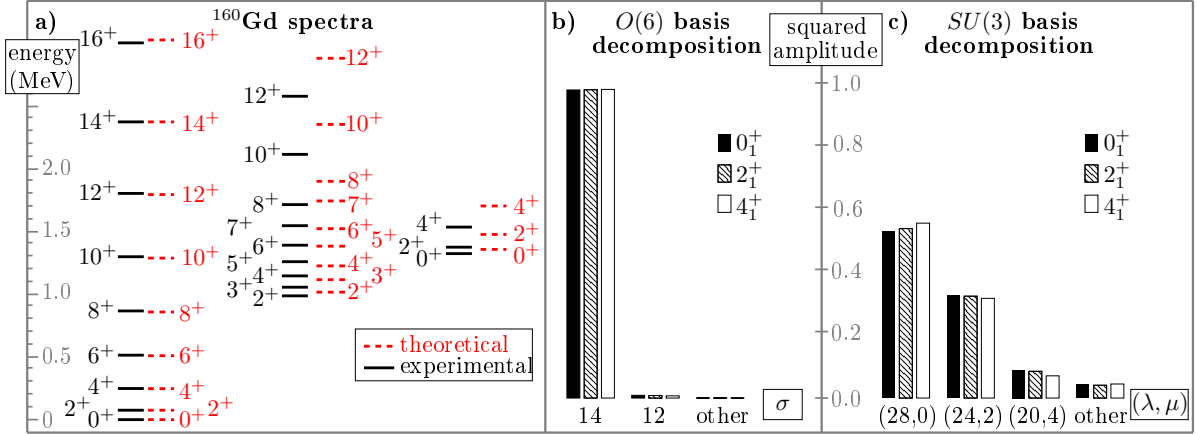


Figure 4. a) The experimental spectrum of ^{160}Gd compared with the IBM calculation using the ECQF Hamiltonian (4) with parameters $\xi = 0.84$ and $\chi = -0.53$ taken from Ref. [21]. b) The $O(6)$ decomposition in σ components of yrast states with $L = 0, 2, 4$. c) The $SU(3)$ decomposition in (λ, μ) components of the same yrast states. Adapted from [12].

equations for $E(\beta, \gamma)$, Eq. (3), $\partial E/\partial\beta = \partial E/\partial\gamma = 0$, have $\beta = 1$ and $\gamma = 0$ as a solution, provided $b = 2c$. For large N , the energy surface coefficients of \hat{H}_{ECQF} are $b = -\omega\xi\sqrt{\frac{2}{7}}\chi/N$ and $c = \omega[1 - \xi - \xi\chi^2/14]/N$. Thus, in the valley of low $\Delta\sigma_0$ the desired condition, $b = 2c$, fixes ξ to be $\xi = 1/[1 - \chi/\sqrt{14} + \chi^2/14]$. This relation predicts the location of the region of approximate ground-state $O(6)$ symmetry for large N very precisely [12]. These results demonstrate that coherent mixing of one symmetry (QDS) can result in the purity of a quantum number associated with partial conservation of a different, incompatible symmetry (PDS).

4. Simultaneous occurrence of $U(5)$ -PDS and $SU(3)$ -QDS in shape-coexistence

PDS (partial purity) and QDS (coherent mixing) of distinct symmetries can occur simultaneously also in different sets of eigenstates of a given Hamiltonian. Such a situation is encountered, for example, in a first-order quantum phase transition (QPT) involving shape coexistence. Focusing on the intrinsic dynamics [22] at the critical-point such QPT between spherical [$U(5)$] and deformed [$SU(3)$] shapes, the relevant IBM Hamiltonian annihilates the corresponding condensates (2) with $\beta = 0$ and $(\beta = \sqrt{2}, \gamma = 0)$, and can be transcribed in the form [23, 24]

$$\hat{H}_{\text{cri}} = h_2 P_2^\dagger \cdot \tilde{P}_2 \quad , \quad P_{2m}^\dagger = 2d_m^\dagger s^\dagger + \sqrt{7}(d^\dagger d^\dagger)_m^{(2)} \quad , \quad \tilde{P}_{2m} = (-)^m P_{2,-m} \quad . \quad (6)$$

\hat{H}_{cri} mixes terms from different DS chains of the IBM, hence is non-integrable. The corresponding classical Hamiltonian, obtained by Glauber coherent states, has a Landau potential with two degenerate spherical and prolate-deformed minima, as shown in Fig. 5. A detailed classical analysis [13–15] reveals a robustly regular dynamics in the region of the deformed minimum and a change with energy from regular to chaotic dynamics in the region of the spherical minimum. The mixed but well separated dynamics persists even at energies far exceeding the barrier height. A quantum analysis is based on Peres lattices [25], which are constructed by plotting the expectation values $x_i \equiv \sqrt{2\langle i|\hat{n}_d|i\rangle/N}$ of the d -boson number operator, versus the energy $E_i = \langle i|\hat{H}|i\rangle$ of the Hamiltonian eigenstates $|i\rangle$. The lattices $\{x_i, E_i\}$ corresponding to regular dynamics display an ordered pattern, while chaotic dynamics leads to disordered meshes of points [25]. The quantity x_i is related to the coordinate x in the classical potential, hence the indicated lattices can distinguish regular from irregular states and associate them with a given region in phase space.

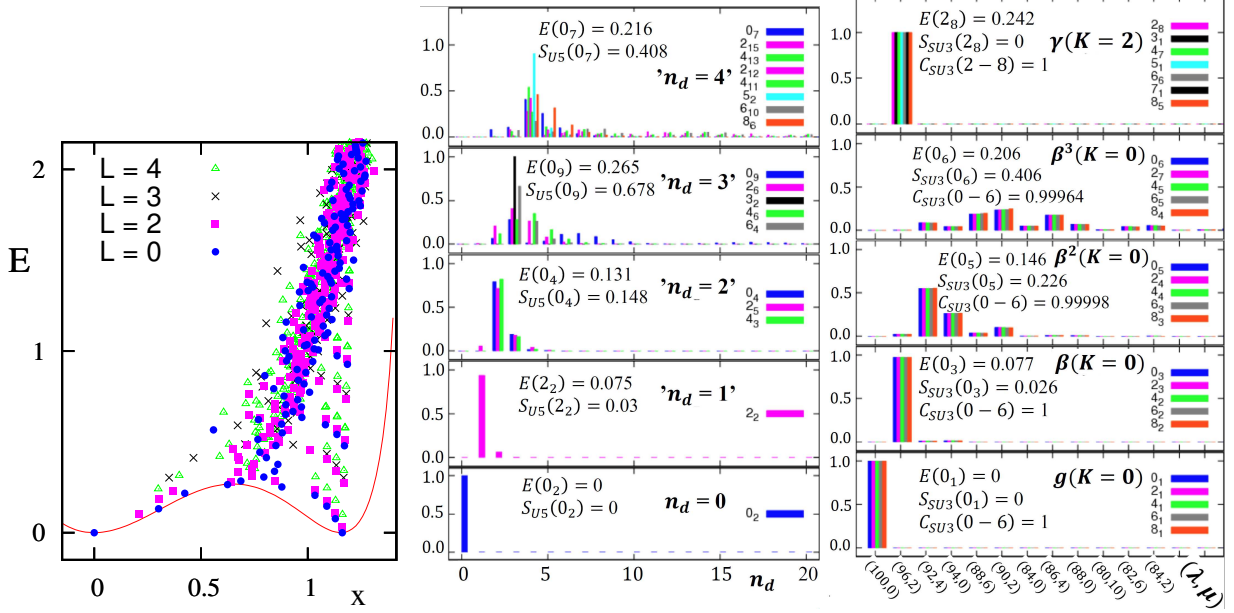


Figure 5. Peres lattices $\{x_i, E_i\}$ for $L=0, 2, 3, 4$ and $N=50$ eigenstates of \hat{H}_{cri} , Eq. (6), overlaid on the classical potential. Here $x_i \equiv \sqrt{2\langle L_i | \hat{n}_d | L_i \rangle / N}$. Adapted from [15].

Figure 6. Left column: U(5) n_d -probability distribution for spherical type of eigenstates of \hat{H}_{cri} , Eq. (6), arranged in U(5)-like n_d -multiplets. Right column: SU(3) (λ, μ) -probability distribution for deformed type of eigenstates arranged in rotational K -bands. Shannon entropies $S_{U5}(L_i) \approx 0$ and $S_{SU3}(L_i) \approx 0$ signal U(5)-PDS and SU(3)-PDS, respectively. SU(3) Pearson correlator $C_{SU3}(0-6) \approx 1$, signals SU(3)-QDS. Adapted from [15].

The Peres lattices for eigenstates of \hat{H}_{cri} (6), with $L=0, 2, 3, 4$, are shown in Fig. 5, overlaid on the classical potential. They disclose regular sequences of states localized within and above the deformed well. They are comprised of rotational states with $L=0, 2, 4, \dots$ forming regular $K=0$ bands and sequences $L=2, 3, 4, \dots$ forming $K=2$ bands. Additional K -bands (not shown in Fig. 5), corresponding to multiple β and γ vibrations about the deformed shape, can also be identified. Such ordered band-structures persist to energies above the barrier and are not present in the disordered (chaotic) portions of the Peres lattice. At low-energy, in the vicinity of the spherical well, one can also detect multiplets of states with $L=0$, $L=2$ and $L=0, 2, 4$, typical of quadrupole excitations with $n_d=0, 1, 2$, of a spherical shape.

The nature of the surviving regular sequences of selected states, is revealed in a symmetry analysis of their wave functions. The left column of Fig. 6 shows the U(5) n_d -probabilities, $P_{n_d}^{(L_i)}$, for eigenstates of \hat{H}_{cri} (6), selected on the basis of having the largest components with $n_d=0, 1, 2, 3, 4$, within the given L spectra. The states are arranged into panels labeled by ' n_d ' to conform with the structure of the n_d -multiplets of the U(5) DS limit. In particular, the zero-energy $L=0_2^+$ state is seen to be a pure $n_d=0$ state, with vanishing U(5) Shannon entropy, $S_{U5}=0$. It is a solvable eigenstate of \hat{H}_{cri} , exemplifying U(5)-PDS [24]. The state 2_2^+ has a pronounced $n_d=1$ component (96%) and the states ($L=0_4^+$, 2_5^+ , 4_3^+) in the third panel, have a pronounced $n_d=2$ component and a low value of $S_{U5} < 0.15$. All the above states with ' $n_d \leq 2$ ' have a dominant single n_d component, and hence qualify as 'spherical' type of states. They are the left-most states in the Peres lattices of Fig. 5. In contrast, the states in the panels ' $n_d=3$ ' and ' $n_d=4$ ' of Fig. 6, are significantly fragmented. A notable exception is the $L=3_2^+$ state, which is a solvable U(5)-PDS eigenstate with $n_d=3$ [24]. The existence in the spectrum of specific spherical-type of states with either $P_{n_d}^{(L)} = 1$ [$S_{U5}(L) = 0$] or $P_{n_d}^{(L)} \approx 1$ [$S_{U5}(L) \approx 0$],

exemplifies the presence of an exact or approximate U(5) PDS at the critical-point.

The states considered in the right column of Fig. 6 have a different character. They belong to the five lowest regular sequences seen in the Peres lattices of Fig. 5, in the region $x \geq 1$. They have a broad n_d -distribution, hence are qualified as ‘deformed’-type of states, forming rotational bands: $g(K=0)$, $\beta(K=0)$, $\beta^2(K=0)$, $\beta^3(K=0)$ and $\gamma(K=2)$. The ground $g(K=0)$ and $\gamma(K=2)$ bands are pure [SU(3) (λ, μ) -distribution, $P_{(\lambda, \mu)}^{(L)} = 1$, and SU(3) Shannon entropy, $S_{\text{SU3}}(L) = 0$] with $(\lambda, \mu) = (2N, 0)$ and $(2N - 4, 2)$ SU(3) character, respectively. These are solvable bands of \hat{H}_{cri} and exemplify SU(3)-PDS [24]. The non-solvable K -bands are mixed with respect to SU(3) in a coherent, L -independent manner, hence exemplify SU(3)-QDS. As expected, the Pearson correlator [26] is $C_{\text{SU3}}(0_i-6) \approx 1$, for these regular K -bands. The above results demonstrate that PDS and QDS can characterize the remaining regularity in a system, amidst a complicated (at time chaotic) environment of other states.

5. Concluding remarks

Both PDS and QDS do not arise from invariance properties of the Hamiltonian, hence can occur simultaneously in atomic nuclei. As shown, the existence of a region of almost exact ground-state-band O(6) symmetry outside the O(6) DS limit of the IBM, can be understood in terms of an approximate O(6) PDS. The same wave functions display coherent (L -independent) mixing of SU(3) irreps and hence comply with the conditions of an SU(3) QDS. Many rare-earth nuclei do exhibit this linkage. Both types of emergent symmetries can characterize persisting regular patterns in nuclei, *e.g.*, U(5)-like and SU(3)-like multiplets, amidst a complicated environment of other states, a situation encountered in a quantum shape-phase transition.

The work reported in Section 3, was done in collaboration with C. Kremer, J. Beller, N. Pietralla, R. Trippel (Darmstadt), G. Rainovski (Sofia), P. Van Isacker (GANIL) and in Section 4, with M. Macek (Yale), and is supported by the Israel Science Foundation.

References

- [1] For a review see, Leviatan A 2011 *Prog. Part. Nucl. Phys.* **66** 93
- [2] Leviatan A 1996 *Phys. Rev. Lett.* **77** 818; Leviatan A and Sinai I 1999 *Phys. Rev. C* **60** 061301
- [3] Leviatan A, García-Ramos J E and Van Isacker P 2013 *Phys. Rev. C* **87** 021302(R)
- [4] Casten R F, Cakirli R B, Blaum K, and Couture A 2014 *Phys. Rev. Lett.* **113** 112501
- [5] García-Ramos J E, Leviatan A and Van Isacker P 2009 *Phys. Rev. Lett.* **102** 112502
- [6] Van Isacker P, Jolie J, Thomas T and Leviatan A 2015 *Phys. Rev. C* **92** 011301(R)
- [7] Couture A, Casten R F, and Cakirli R B 2015 *Phys. Rev. C* **91** 014312
- [8] Escher J and Leviatan A 2000 *Phys. Rev. Lett.* **84** 1866; *ibid* 2002 *Phys. Rev. C* **65** 054309
- [9] Van Isacker P and Heinze S 2008 *Phys. Rev. Lett.* **100** 052501; *ibid* 2014 *Ann. Phys. (NY)* **349** 73
- [10] Bahri C and Rowe D J 2000 *Nucl. Phys. A* **662** 125
- [11] Rowe D J 2004 *Nucl. Phys. A* **745** 47; Rosensteel G and Rowe D J 2005 *Nucl. Phys. A* **759** 92
- [12] Kremer C, Beller J, Leviatan A, Pietralla N, Rainovski G, Trippel R, and Van Isacker P 2014 *Phys. Rev. C* **89** 041302(R); *ibid* 2015 *Phys. Rev. C* **92** 039902(E)
- [13] Macek M and Leviatan A 2011 *Phys. Rev. C* **84** 041302(R)
- [14] Leviatan A and Macek M 2012 *Phys. Lett. B* **714** 110
- [15] Macek M and Leviatan A 2014 *Ann. Phys. (NY)* **351** 302
- [16] Iachello F and Arima A 1987 *The Interacting Boson Model* (Cambridge: Cambridge Univ. Press)
- [17] Ginocchio J N and Kirson M W 1980 *Phys. Rev. Lett.* **44** 1744
- [18] Warner D D and Casten R F 1983 *Phys. Rev. C* **28** 1798
- [19] Casten R F and Warner D D 1983 *Prog. Part. Nucl. Phys.* **9** 311
- [20] Kremer C 2015 private communication
- [21] McCutchan E A, Zamfir N V and Casten R F 2004 *Phys. Rev. C* **69** 064306
- [22] Leviatan A 1987 *Ann. Phys. (NY)* **179** 201; Leviatan A and Kirson M W 1990 *Ann. Phys. (NY)* **201** 13
- [23] Leviatan A 2006 *Phys. Rev. C* **74** 051301(R)
- [24] Leviatan A 2007 *Phys. Rev. Lett.* **98** 242502
- [25] Peres A 1984 *Phys. Rev. Lett.* **53** 1711
- [26] Macek M, Dobeš J and Cejnar P 2010 *Phys. Rev. C* **82** 014308